19th Brazilian Congress of Thermal Sciences and Engineering
November 06th-10th, 2022, Bento Gonçalves - RS - Brazil

ENC-2022-0167
EVALUATION OF THE WSGG MODEL FOR COUPLED CALCULATIONS OF LAMINAR FLAMES

Pedro Wink Guaragna
Guilherme Crivelli Fraga
Francis Henrique Ramos França
Department of Mechanical Engineering, Federal University of Rio Grande do Sul, 425 Sarmento Leite St., Porto Alegre, Brazil
pedro.guaragna@ufrgs.br
guilhermecfraga@gmail.com
frfrança@mecanica.ufrgs.br

Abstract. *The abstract should describe the objectives, the methodology and the main conclusions of the paper in about 200 words. It should not contain neither formulae nor reference to bibliography Combustion gases emit and absorb radiation in a wide range of temperatures however, they do not so continuously regarding the wavelength. Different approaches were developed over the years to replicate this phenomenon, the most widely spread one perhaps being the weighted-sum-of-gray-gases (WSGG), that models the absorption behavior of the real gas as combination of a small number of gray gases. Most works in literature assess the WSGG model by evaluating the radiative heat transfer equation decoupled from the combustion and fluid flow processes, i.e. where the radiation field is computed from predetermined fields of pressure, temperature and species concentration. In practical applications, though, radiation is coupled to all other physical processes, and it is known that inaccuracies in the prediction of the radiation field can lead to errors in other scalars, such as the temperature and the rate of species formation. Therefore, this study carries out an evaluation of different formulations of the WSGG model for coupled radiation-combustion calculations of a set of one-dimensional, laminar flames. The calculations are performed in the CHEM1D code, on which the WSGG model (and the line-by-line integration method, which serves as the benchmark for the comparisons) has been implemented.*

Keywords: *combustion, thermal radiation, WSGG, flamelet*

1. INTRODUCTION

The radiative heat transfer process in participating media is a subject of great importance, especially for the energy generation industry, as in combustion processes thermal radiation is generally the main heat transfer mode. However, its reliable computation still is challenging. The radiative properties of absorbing-emitting species have a complex behavior as these are not regularly distributed regarding the wavelength, but rather in specified intervals, called bands, inside which they strongly oscillate. Moreover, radiation in participating media is a volumetric phenomenon, instead of a surface phenomenon, so changes in the temperature and species concentration of the gases throughout space must also be accounted for. Compromise between accuracy and computational costs must be accounted for when modelling the gas radiation in the combustion process.

The high gradient of temperature and species concentration participating in the heat transfer presents problems of numerical convergence. And as mentioned before, for each wavelength of a participating gas there are millions of spectral lines to represent the radiative behavior. The most accurate solution for spectral aspect of a participating gas can be achieved by the line-by-line integration (LBL) of each wavenumber of the spectrum. This method is considered as the benchmark results as it is almost exact minor some deviations due to approximations in the calculation.

The weighted-sum-of-gray-gases (WSGG) model approximates the behavior of a gas by representing its spectrum with a few gray gases that occupy certain noncontiguous portions of the spectrum plus a transparent window. The absorption and emission-weighting coefficient associated to each gray gas must be determined, with different works in literature developing iterations of this model with fitting data, usually total emittances, based upon different scenarios. One of the most widely referred work is by Smith et al., 1982, where coefficients were fitted against emittance data computed from exponential wide-band model for typical combustion products of methane and fuel oil. For these fuels, the corresponding partial pressure ratios between water vapor and carbon dioxide are 2/1 and 1/1, respectively.

Other authors also developed correlations for the WSGG model, including Selhorst et al., 2020, that proposed new coefficients that accounted for variations of the molar ratio in the domain based on the up-to-date HITEMP2010 spectral database and validated the results with line-by-line (LBL) integration for one and three-dimensional cases whereas for cases with higher gradients of temperature and molar ratio the error was below the 15%.

In most cases, the validation and development of the WSGG correlations were made in decoupled calculations of the radiative transfer equation, where temperature and molar concentration data were predefined, either from experimental data or from empirical distribution. In real combustion applications, however, radiation is coupled to all other physical processes, and it thus affects scalars such as the temperature and the reaction rates and formation of species, as well as the propagation speed and extinction characteristics. On the other hand, changes in the afore mentioned scalars influence the radiative properties of the medium and, as consequence, on the resulting radiation field.

Due to computational costs, spatially demanding simulations of flames are a challenge, the more so if coupled with the RTE. The CHEM1D software developed by Somers, 1994, which solves one dimensional flame structures known as flamelets, proves a powerful tool for solving detailed chemistry flames coupled with the radiative problem. These flamelets represent the transport, chemical kinetics and radiative heat transfer decoupled from flow equations.

Therefore, the purpose of the present study is to evaluate different propositions of the WSGG model and compare them with the LBL method regarding the results calculated for the fields of temperature and species concentration, as well as the radiation field. Cases simulated are focused on methane and air combustion, with or without dilution of CO_2 in the fuel. Besides these methods, comparisons with calculations that neglect radiation or use the optically thin approximation to account for the radiative transfer are also performed. This work focused its research on counterflow flames, as represented in Figure (1):

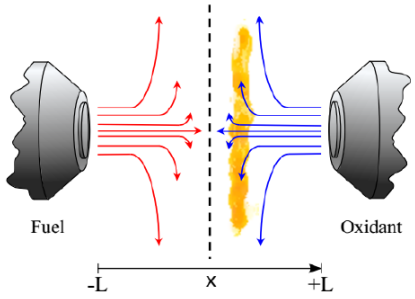

Figure 1: Counterflow flame.

2. RADIATIVE TRANSFER EQUATION AND SPECTRAL MODELLING

Determination of the radiation field in participating media requires the solution of the radiative transfer equation (RTE). For a medium that absorbs and emits radiation, but where scattering is neglected, the RTE is given as (Howell et al., 2016):

$$\frac{dI_\eta(S)}{dS} = -\kappa_\eta(S)I_\eta(S) + \kappa_\eta(S)I_{b\eta}(S) \tag{1}$$

where $I_\eta(S)$ and $I_{b\eta}(S)$ are, respectively, the spectral intensity and the blackbody spectral intensity at position S along a given path. The term κ_η stands as the spectral absorption coefficient. It should be noted that η stands for wavenumber. Considering a gas with uniform conditions of temperature and composition, for example, a well-mixed furnace, then κ_η and $I_{b\eta}$ are constant throughout the volume and integration of Eq. (1) from *0* to *S* will yield:

$$I_\eta(S) = I_\eta(0)e^{-\kappa_\eta S} + I_{b\eta}[1 - e^{-\kappa_\eta S}] \tag{2}$$

where $e^{-\kappa_\eta S}$ stands for the spectral transmittance. The integration of the RTE over all the spectrum will result in the total absorptance along the uniform path:

$$\alpha(S) = \frac{\int_0^\infty I_\eta(0)\alpha(S)d\eta}{\int_0^\infty I_\eta(0)d\eta} = \frac{\int_0^\infty I_\eta(0)\left[1-e^{-\kappa_\eta S}\right]d\eta}{\int_0^\infty I_\eta(0)d\eta} \tag{3}$$

It is more convenient, in order to evaluate the absorptance of the gas, to consider the integral of Eq. (3) in terms of a single broadened line η_{ij} where, therefore, the absorption coefficient κ_{ij} is essentially null except in a narrow wavenumber range surrounding this single line. The intensities $I_\eta(0)$ and $I_{b\eta}$ remain essentially constant within this range. The integration becomes:

$$\alpha_{ij}(S) = \frac{I_{\eta_{ij}}(0)\int_{-\infty}^{\infty}\{1-exp[-\kappa_{\eta,ij}S]\}d(\eta-\eta_{ij})\eta}{\int_0^{\infty} I_\eta(0)d\eta} \quad (4)$$

Also, of importance in the validation of models for participating media, is the definition of the total emittance. This solution is for an absorbing gas "*a*" that is mixed with other gases "*r*", non-participating, in an isothermal (with value of *T*), homogeneous media along the path *S*:

$$\varepsilon_a(T,p_a\cdot S) = \frac{\int_{\eta=0}^{\infty} I_{\eta b}(\eta,T)\cdot 1 - e^{(-\kappa p\eta,a\cdot p_a\cdot S)}d\eta}{\sigma T^4/\pi} \quad (5)$$

where $I_{\eta b}$ is the spectral intensity of radiation of the black body (given by the Planck distribution):

$$I_{\eta b}(\eta,T) = \frac{2C_1\eta^3}{exp(C_2\eta/T)-1} \quad (6)$$

in which C_1 is the first Planck's constant, equal to 0.59552137×10^{-12} Wcm^2/sr.

2.1 The Discrete Ordinates Method (DOM)

In order to integrate the spatial domain, the discrete ordinates method was applied, although it should be noted that the WSGG can be solved with any other method of solving the spatial domain. The method of the Discrete Ordinate Method (DOM) was originally proposed by Chandrasekhar, 1960, and is based upon the discrete representation of the directional dependence of the radiation intensity. In this way, the RTE is solved for a set of directions that cover in their entirety the extension of the 360 degrees (for a one-dimensional case, and for the three-dimensional case the solid angle) [Modest, 2003].

In the conditions of this work, where the participating media is bounded by two parallel surfaces that have black body properties and set at the constant temperature of 298 K. The method solves the spectral intensity in a forward, $I_{i,l}^{+}(s)$, and a backward $I_{i,l}^{-}(s)$, direction, as depicted in Figure (2) with the resulting RTE having the form:

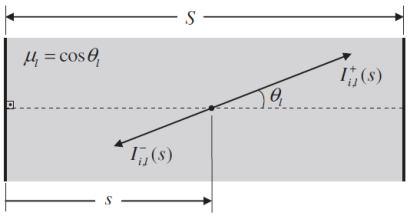

Figure 2. Schematic of the one-dimensional domain. Adapted from Dorigon et al., 2013

$$\mu_l \frac{\partial I_{\eta,l}^{+}(x)}{\partial x} = -\kappa_\eta(x) I_{\eta,l}^{+}(x) + \kappa_\eta(x) I_{b,\eta}(x) \quad (7a)$$

$$-\mu_l \frac{\partial I_{\eta,l}^{-}(x)}{\partial x} = -\kappa_\eta(x) I_{\eta,l}^{-}(x) + \kappa_\eta(x) I_{b,\eta}(x) \quad (7b)$$

where μ_l represents the cosine of angle θ_l and $I_{\eta,l}^{+}$ and $I_{\eta,l}^{-}$ are the radiation intensity in the forward and backward direction for $\mu_l > 0$ and, $\mu_l < 0$ respectively.

Equation (7) is a set of first order linear equations dependent on $I_{\eta,l}(x)$, thus, it only requires one boundary condition for each equation. This requirement is fulfilled by assuming that the walls of the domain behave like a blackbody, and therefore the fulfilling condition can be written as:

$$I_{\eta,l}^{+}(x=0) = I_{b,\eta}(x=0) \quad (8a)$$

$$I_{\eta,l}^{-}(x=X) = I_{b,\eta}(x=X) \quad (8b)$$

After solving Eqs. (7a) and (7b), one can calculate the net radiative heat flux and volumetric source in position s, respectively through the equations:

$$q_R''(s) = \sum_{i=0}^{I} \sum_{l=1}^{L} 2\pi\mu_l w_l \left[I_{i,l}^{+}(s) - I_{i,l}^{-}(s) \right] \tag{9a}$$

$$\dot{q}_R(s) = \sum_{i=0}^{I} \sum_{l=1}^{L} 2\pi w_l \kappa_{p,i} p_a(s) \left\{ \left[I_{i,l}^{+}(s) + I_{i,l}^{-}(s) \right] - 2a_i(s) I_b(s) \right\} \tag{9b}$$

in which w_l is the quadrature weight for l direction. An important direct consequence of the Equations (7) and (9) is that the WSGG model is intrinsically conservative since the radiative energy balance is satisfied as $\dot{q}_R(s) = -dq_R''(s)/ds$. This factor is crucial when radiation is coupled with other heat transfer mechanisms in the global energy equation.

2.2 The line-by-line integration

The line-by-line (LBL) method usually stands as the benchmark solution due to the accuracy that can be achieved by performing a discretization on the wavenumber until a well-established convergence criterion. This high accuracy is product of solving the RTE for each absorption coefficient related to its respective wavenumber. However, since the databases from which the spectral properties are computed, are obtained through experimental methods, the obtention process itself gather some errors and therefore the LBL solution are not exact.

After solving the RTE using Equation (7), the radiative heat flux, and radiative heat source can be obtained:

$$q''(x) = \sum_{l=1}^{L} \int_{\eta=0}^{\infty} \left\{ 2\pi\mu_l g_l \left[I_{\eta,l}^{+}(x) - I_{\eta,l}^{-}(x) \right] \right\} d\eta \tag{10a}$$

$$-\nabla q''(x) = \sum_{l=1}^{L} \int_{\eta=0}^{\infty} \left\{ 2\pi g_l \kappa_\eta \left[I_{\eta,l}^{+}(x) + I_{\eta,l}^{-}(x) \right] - 4\pi\kappa_\eta I_{\eta,b}(x) \right\} d\eta \tag{10b}$$

where g_l is the quadrature weight in the l direction.

2.3 The weighted-sum-of-gray-gases (WSGG) model

The WSGG model represents the spectrum in its entirety with only a few gray gases with a uniform pressure absorption coefficient, plus a transparent window. The model assumes that the *i*th gas covers a fixed, noncontiguous portion of the spectrum, $\Delta\eta_i$ and that the pressure absorption coefficient $\kappa_{p,i}$ is independent of the temperature T and of the partial pressure p_a of the participating species. Both considerations serve as a stricter form of scaling approximation, as in this way, the dependence the absorption coefficient has on the wavenumber and on the thermodynamic state (temperature and molar concentrations) are decoupled.

Integrating Eq. (5) over the spectrum with the WSGG model, the total emittance becomes:

$$\varepsilon\left(T, p_a \cdot S\right) = \sum_{i=1}^{I} a_i(T) \left[1 - exp\left(-\kappa_{p,i} p_a S \right) \right] \tag{11}$$

in which $a_i(T)$ is the fraction of the blackbody emission in the range of the spectrum corresponding to the *i*th gray gas, as determined from the fitting.

The parameters from WSGG that are calculated from the fitting expression can be used to solve general radiation problems, not being limited only to isothermal, uniform medium. This fitting to emittance data with Equation (11) allows obtaining the pressure absorption coefficients $\kappa_{p,i}$ of each gray gas as well as the temperature dependent coefficients $a_i(T)$ which can be represented by polynomial functions:

$$a_i(T) = \sum_{j=1}^{J} b_{i,j} T^j \tag{12}$$

in the above equation, $b_{i,j}$ is the polynomial coefficient of *j*th order for the *i*th gray gas.

The temperature dependent coefficients are calculated as above only for the gray gases, in order for the radiation energy to remain conserved, and so the transparent window is calculated as:

$$a_o(T) = 1 - \sum_{i=1}^{I} a_i(T) \tag{13}$$

The determination of these coefficients varies from author to author with each using the fitting data that best responded to their benchmark comparisons. As part of the simplification proposed by the WSGG, the total radiation intensity in a certain direction is computed by the summation of the intensities I_i related to each gray gas:

$$I(S) = \sum_{i=1}^{I} I_i(S) \tag{14}$$

where this partial intensity I_i can be obtained through integration, as mentioned above, of Equation (1) applied to a single gray gas:

$$\frac{dI_i(S)}{dS} = -\kappa_{p,i} p_a(S) I_i(S) + \kappa_{p,i} p_a(S) a_i(S) I_b(S) \tag{15}$$

in which $p_a(S)$ is the partial pressure of the participating species, $a_i(S)$ is the temperature dependent coefficient and $I_b(S)$ is the total intensity of the blackbody evaluated at local conditions (at position S).

Therefore, although the WSGG model assumes that the pressure absorption coefficient is constant, the temperature dependent coefficient and the partial pressure terms can account for changes in temperature and molar concentrations, allowing the application of the model in non-isothermal, non-homogeneous media. Again, using the DOM for solving the spatial directions, Equation (7) becomes:

$$\mu_l \frac{\partial I_{i,l}^{+}(x)}{\partial x} = -\kappa_{p,i} p_a(x) I_{i,l}^{+}(x) + \kappa_{p,i} p_a(x) a_i(x) I_b(x) \tag{16a}$$

$$-\mu_l \frac{\partial I_{i,l}^{-}(x)}{\partial x} = -\kappa_{p,i} p_a(x) I_{i,l}^{-}(x) + \kappa_{p,i} p_a(x) a_i(x) I_b(x) \tag{16b}$$

As previously stated, the walls are considered blackbodies, and the boundary conditions undergo a small change to adapt for the model. The conditions become:

$$I_{i,l}^{+}(x=0) = a_i(T_{x=0}) I_b(x=0) \tag{17a}$$

$$I_{i,l}^{-}(x=X) = a_i(T_{x=X}) I_b(x=X) \tag{17b}$$

Like the LBL integration, after solving the Equation 16, the radiative heat flux and radiative heat source can be calculated [Howell et al., 2016]:

$$q''(x) = \sum_{l=1}^{L} \sum_{i=0}^{I} \left\{ 2\pi \mu_l g_l \left[I_{i,l}^{+}(x) - I_{i,l}^{-}(x) \right] \right\} \tag{11a}$$

$$-\nabla q''(x) = \sum_{l=1}^{L} \sum_{i=1}^{I} \left\{ 2\pi g_l \kappa_{p,i} p_a(x) \left[\left[I_{i,l}^{+}(x) + I_{i,l}^{-}(x) \right] - 2 a_i I_b(x) \right] \right\} \tag{11b}$$

The same as with the LBL, the energy balance is assured. Also of importance, the transparent window, $i = 0$, is only accounted for when obtaining the radiative heat flux.

3. NUMERICAL METHOD AND WORK METHODOLOGY

The CHEM1D software solves the transport equations for the conservation of mass, conservation of chemical species and conservation of energy according to the flamelet formulation proposed by de Goey *et al.*, 1999, with assumptions of laminar flame and low Mach number. Since the calculations are for one-dimensional analysis, a stretch rate K is introduced to account for the effects of multidimensionally not present in the 1D scenario, whose conservation equation is written as:

$$\frac{\partial(\rho u K)}{\partial x} = \frac{\partial}{\partial x}\left(\mu \frac{\partial K}{\partial x}\right) - \rho K^2 + (\rho a^2)_{ox} \tag{14}$$

in which ρ is the specific mass, u is the velocity in the x direction, μ is the dynamic viscosity of the mixture and the term a here stands for the strain rate at the oxidant side, and is written as:

$$a = -\frac{\partial u}{\partial x} \tag{15}$$

this represents the velocity gradient of the flow. When solving the radiative transfer equation, the software brings as input for it the temperature and molar fractions of water vapor and carbon dioxide, as well the position of each volume in the discretization scheme. As an output from the RTE, the result for the radiative volumetric source is added to energy balance equation.

The detailed mechanism DRM19 proposed by Kazakov et al., 1995, which consists of 19 species was used for the chemical kinetics. As noted by Goswami, 2014, this mechanism can show up to 11% in deviations of burning velocity if compared to more detailed mechanism like GRI Mech 3.0 (which consists of 53 species). However, more species inevitable results in higher calculation costs.

Therefore, the simulation settings were of a counterflow flame, with stationary solution, detailed chemistry model, constant Lewis's diffusion model.

3.1 Mesh convergence

To ensure that results were not affected by computational errors due to the discretization of the problem, a study regarding the quality of mesh was performed. Three different meshes were applied, M1, M2 and M3 which had respectively, 400, 200 and 100 volumes each. Values to determine the mesh quality were the maximum values of temperature, velocity, and carbon monoxide. Other results, such as species for water vapor and carbon dioxide, were also included in this analysis but there was no noticeable difference in their formations.

The methodology for mesh analysis was the Grid Convergence Index (GCI), first presented by Roache, 1994 and updated by Celik et al., 2008 and will be briefly discussed. The main purpose of the GCI is to report the results of the mesh convergence study uniformly and present an estimation of the error related to the solution. Although it can be calculated with two set of meshes, ideally should be used three meshes to estimate if the results are within an asymptotic curve of convergence. Therefore, the GCI is an estimation of the calculated results and the asymptotic value of a mesh with infinite number of volumes. The results are presented in Table 1.

Table 1. GCI and convergency factor.

	T_{max}	V_{max}	$X_{H2O,max}$	$X_{CO2,max}$	$X_{CO,max}$
GCI_{12} [%]	5.85×10^{-5}	2.01×10^{-2}	1.24×10^{-4}	2.24×10^{-3}	1.30×10^{-5}
GCI_{23} [%]	7.80×10^{-6}	4.04×10^{-2}	1.65×10^{-4}	2.94×10^{-3}	1.24×10^{-4}
χ	1.0001	1.0160	1.0000	1.0006	0.9999

The χ is a comparison between the two results of the GCI in which, the closer it is to unity, it indicates that the solution is closer to the asymptotic range of convergence Therefore, all values presented good results for the mesh convergence study. Although the higher results were with the maximum velocity, with a 2% estimated difference to mesh independence result, the main factors in this study relate to temperature and species concentration as they have direct influence in the radiative heat transfer.

3.2 Work Methodology

The software CHEM1D was available already with the Optically Thin Approximation (OTA) as option for radiative modeling. However, the tool is very accessible in terms of user customization and therefore the present work has endeavored in the adapting the in-house Fortran codes for solving the RTE via LBL and WSGG into the source code of the software.

In total it was implemented 14 different sets of coefficients for the WSGG model and each of these variations were validated with the in-house code and reviewed according to the available literature. From these three sets were selected (with one of them having two variations, totalizing four models) and were applied in the calculations of a counterflow methane-air combustion.

Altogether, for each radiation model applied, cases were calculated for a varying of strain rate values, with them being 5, 10, 20, 30, 40, 50 and 60 s^{-1}. Also, cases were calculated with CO_2 dilution in the fuel side, going from 0 to 50%. The four different formulations of the WSGG selected for comparison in this work were the ones proposed by: Yin et al., 2013, that has coefficients for molar ratios 1:1 and 2:1; Coelho et al., 2017 and Selhorst et al., 2020.

3.3 WSGG Formulations

The formulation used by Yin et al., 2013, the coefficients are established for a certain molar ratio and does not account for variations of it neither in the pressure absorption coefficient nor in the temperature dependence coefficient. The formulation by Selhorst et al., 2020 accounts for these variations in the temperature dependence coefficient by means of a polynomial curve fitting with the correlations. Finally, the one proposed by Coelho et al., 2017 applies the "superposition" method which calculates individually the pressure absorption and temperature dependence coefficients for water vapor and carbon dioxide and then combines the results. The resulted coefficients are then applied to the calculations of radiative heat source and flux.

4. RESULTS AND DISCUSSION

The first section presents the results for a case of strain rate of 20 s^{-1} and no addition of carbon dioxide while the second shows the effects of decreasing the strain rate and the third of dilution the fuel with CO_2. Section four is an overview of the results for a wide range of strain rates and section five is an overview of fuel dilution.

4.1 Results for 20 s^{-1} strain rate and 0% dilution

Figure 3a shows the results of the temperature field and the concentration of the two participating species and carbon monoxide for the case coupled with the LBL integration while Figure 3b presents the radiative heat source for this method compared to the WSGG formulations. The model with the lowest error for the maximum absolute value of the radiative heat source was Yin2013-MR2 which has an error of around 1.2%. Also, when accounting the whole domain, and for simplicity considering a transversal section of 1 cm^2, it is possible to calculate a net radiative heat loss. When analyzing this property, this model has the accuracy of 7.0%.

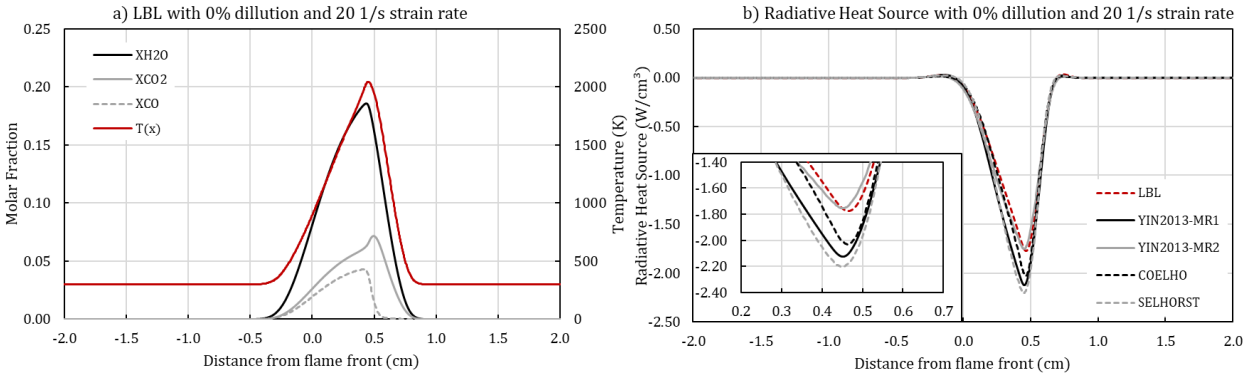

Figure 3. For 20 s^{-1} strain rate and 0% dilution: (a) temperature and main species molar fraction; (b) radiative heat source.

It should be noted that for all cases the domain was set as going from -4 cm to 4 cm, but with the purpose of better visualization, the results are shown only from -2 to 2 cm as this is the region with the presence of gradients of the properties. It wasn't perceived significant differences for water vapor and carbon dioxide (all results below 0.3%), however for temperature and CO formation it was seen difference between methods. Table 2 presents the results for the LBL and the error each model has when compared to the benchmark. It should be remarked that these are not in absolute value, therefore a negative error represents that the model underestimates the result by the LBL integration.

Table 2. Results for a strain rate of 20 s^{-1} and 0% dilution.

Model / Method	T_{max}	$\dot{Q}_{max}$	Q_{total}	$X_{CO,max}$
LBL	2044 K	1.775 W/cm^3	0.0745 W	0.0426
Yin MR1	2035 K	19.6%	23.2%	-2.2%
Yin MR2	2042 K	-1.2%	7.0%	-0.4%
Coelho	2040 K	14.3%	8.4%	-0.9%
Selhorst	2034 K	24.0%	22.0%	-2.3%

Quite interestingly it seems the main factor to affect (and in turn be affected) the radiative properties is the temperature. The two models with closer results to the benchmark also have more accurately predicted the maximum temperature.

4.2 Results for 20 s^{-1} strain rate and 50% dilution

Similar to the previous section Figure 4a illustrates the species concentration while Figure 4b is the comparative of the heat loss of the flame due to the radiation. The model "Yin2013-MR2" is the one with the highest associated error in comparison to the LBL. This result is expected as this simulated case has a higher presence of CO_2 and therefore is further from the specified molar ratio. One of the models best suited for this scenario was the one with the formulation proposed by Selhorst et al., 2020, that has a maximum value error of 3.4%.

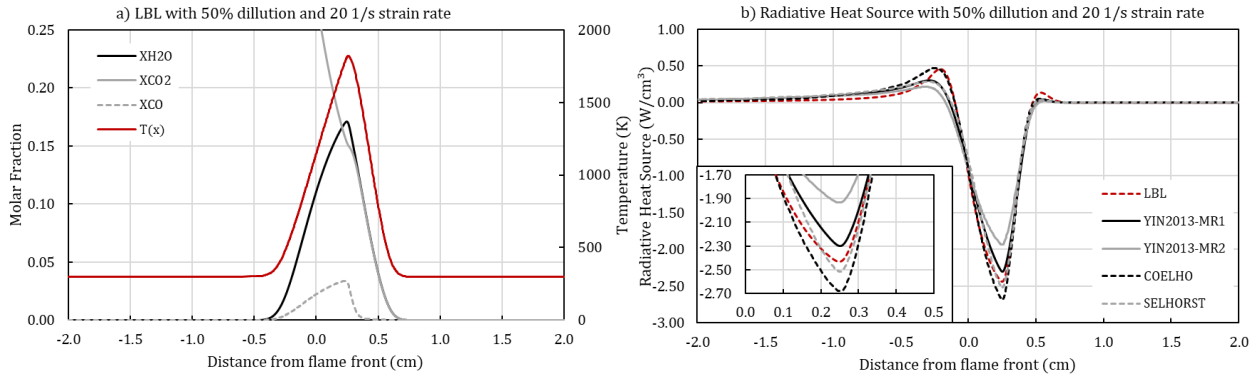

Figure 4. For 20 s^{-1} strain rate and 50% dilution: (a) temperature and main species molar fraction; (b) radiative heat source.

However, observing Figure 4b in the zone with the highest gradients of temperature and species (around the -0.5 and 0 cm) there is an absorption effect caused by the participating species as shown by the LBL result. The model that best described this behavior was the "Coelho" and this effect can be seen in the result of the total radiative heat loss as this method has achieved the lowest inaccuracy with 6.4%. Table 3 presents the results for the LBL and the error each model has when compared to the benchmark.

Table 3. Results for a strain rate of 20 s^{-1} and 50% dilution.

Model / Method	T_{max}	$\dot{Q}_{max}$	Q_{total}	$X_{CO,max}$
LBL	1820 K	2.433 W/cm^3	0.0738 W	0.0336
Yin MR1	1822 K	-5.4%	-16.2%	0.6%
Yin MR2	1829 K	-20.4%	-19.9%	2.4%
Coelho	1815 K	10.2%	-6.8%	-1.0%
Selhorst	1820 K	3.4%	-17.7%	0.2%

Again, it is possible to view the iterative relation between temperature and heat loss, as the model that best predicts the temperature is the same for the maximum radiative heat loss.

4.3 Results for 5 s^{-1} strain rate and 0% dilution

Figure 5a presents the concentration of species and the temperature. Because the strain rate was decreased the flame is naturally more stretched, which can be seen by the gradients that are lower. Figure 5b compares the results of radiative heat source of the four models with the benchmark. Again, reciprocating the case presented for a higher strain rate, the model that has the lowest error is the "Yin-MR2" as this case as similar molar ratio of water vapor and carbon dioxide although as the flame is more stretched it has more overall formation of these species.

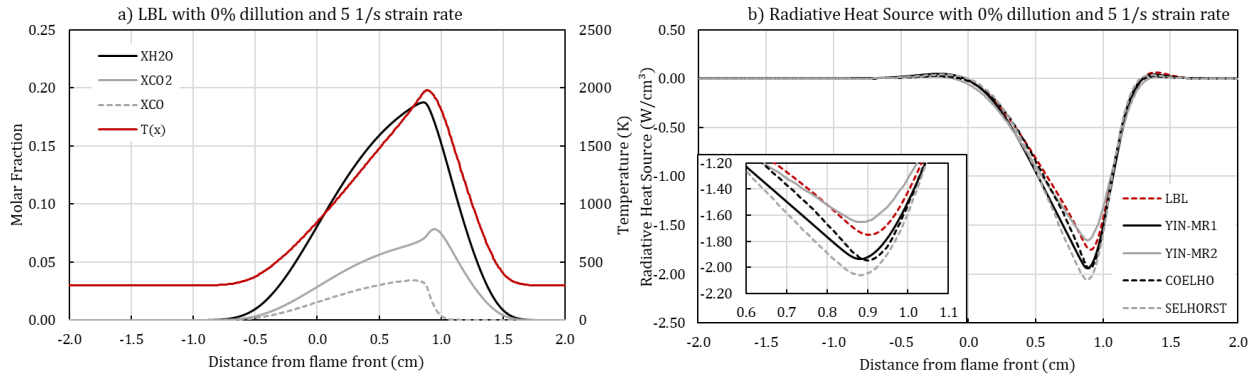

Figure 5. (a) temperature and main species molar fraction; (b) radiative heat source.

Table 4 presents the results for this set up case. Except for the previously mentioned model, the results achieved have improved compared to higher strain rate. However, this is because all models have in general lowered their predicted and as the "Yin-MR2" was already lower than the LBL result, this difference was made wider.

Table 4. Results for a strain rate of 20 s^{-1} and 0% dilution.

Model / Method	T_{max}	$\dot{Q}_{max}$	Q_{total}	$X_{CO,max}$
LBL	1979 K	1.751 W/cm^3	0.1235 W	0.0342
Yin MR1	1961 K	10.6%	13.5%	-5.8%
Yin MR2	1976 K	-5.6%	5.4%	-0.9%
Coelho	1968 K	11.0%	7.3%	-0.9%
Selhorst	1957 K	17.5%	14.5%	-6.9%

4.4 Results for different dilutions of CO_2

This section compiles the results from each model for different dilutions of carbon dioxide and compares their accuracy to the benchmark as function of the dilution. Figure 6 presents the formation of carbon monoxide as term of the maximum value of the molar fraction. All models appear to correctly predict the behavior of this quantity.

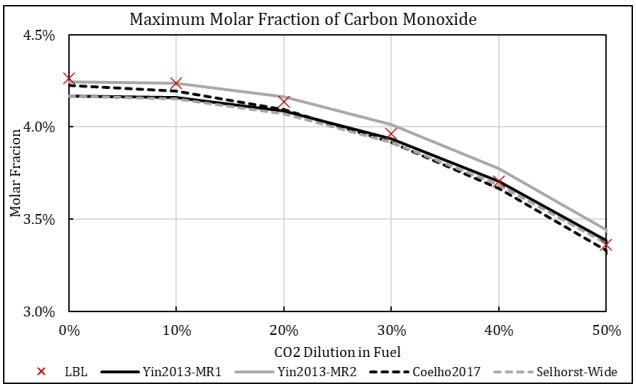

Figure 6. Formation of Carbon Monoxide as function of CO_2 dilution.

Figure 7a illustrates the radiative heat source in terms of maximum value (lowest value of the radiative heat source). It can be noted that the two formulations with fixed molar ratios have a roughly unchanging value as carbon dioxide is added while the two other formulations that account for changes in this variable can better follow the behavior of increasing the maximum value with the more dilution.

On the other side, the Figure 7b shows the radiative heat loss in total for the domain. The results seem to indicate that there is a minimum value of this quantity at a small addition of CO_2 and after that the value returns to increase. For this parameter, the model that best represented this quantity was the one with the superposition method.

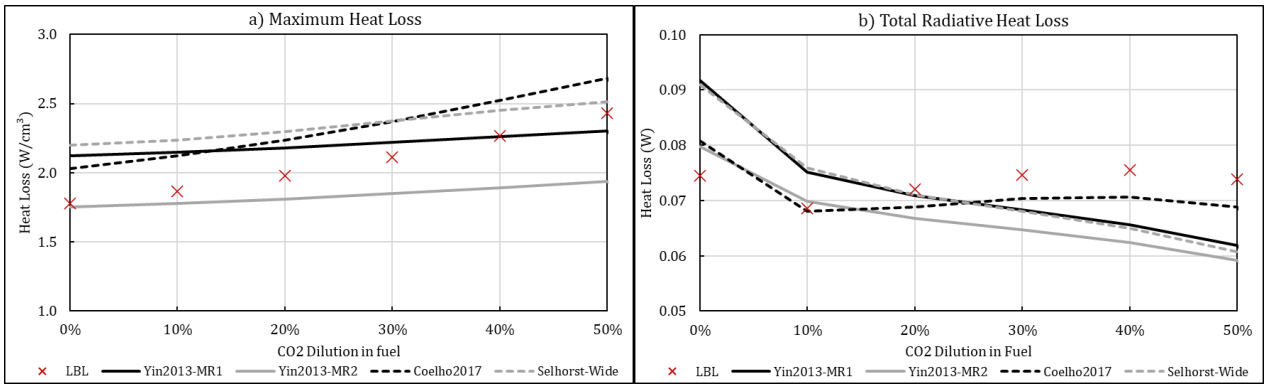

Figure 7. Radiative Heat Loss as function of CO_2 dilution, calculated as (a) maximum value; (b) total value.

4.5 Results for different strain rates

This section is dedicated to an aggrupation of the results as function of the strain rate. Figure 8 presents the formation of carbon monoxide. The Figure seems to indicate that all tested models can acutely predict this quantity with even more accuracy as the strain rate increases and the gradients for the formation of species as well.

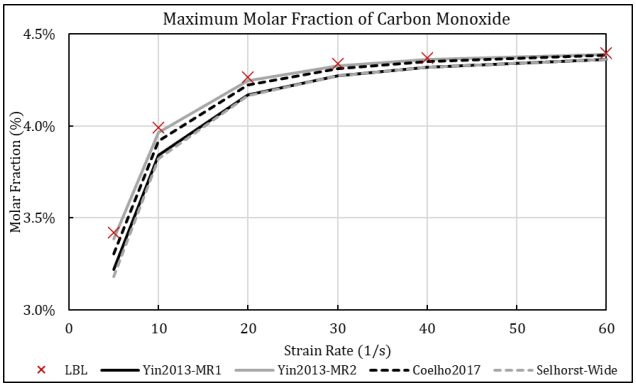

Figure 8. Formation of Carbon Monoxide as function of strain rate.

Figure 9a shows that the model that best predicted the results of the LBL for the maximum radiative heat loss was the "Yin-MR2". This might be since all these compiled cases of varying strain rate have an average molar ratio of 2 to 1. Figure 9b illustrates that as increasing the strain rate, the total radiative heat loss becomes less prevalent in the energy balance of a flame. Also, it can be noted that the models can predict this decrease.

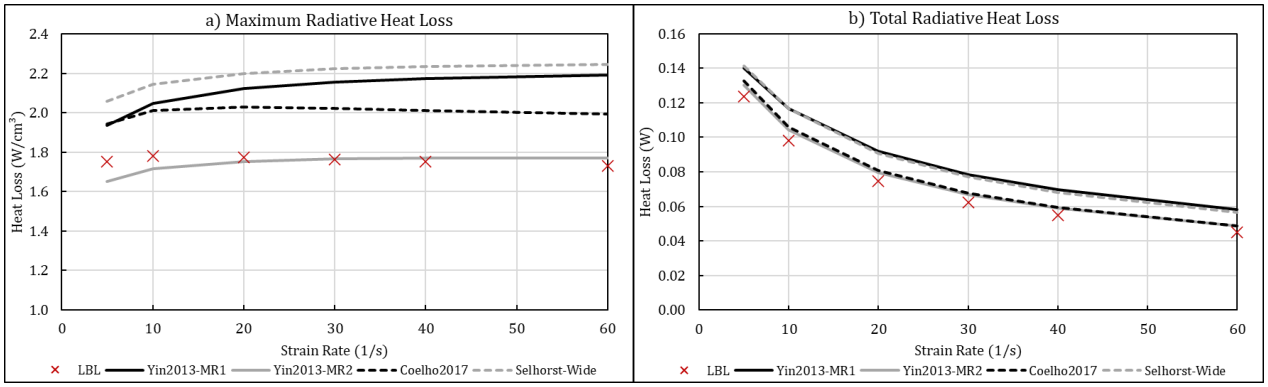

Figure 9. Radiative Heat Loss as function of strain rate, calculated as (a) maximum value; (b) total value.

5. CONCLUSIONS

This paper presented an analysis of the accuracy of different formulations of the WSGG model based on coupled calculations carried out for laminar, counterflow flames. All comparisons were relative to the benchmark solution produced by the LBL integration of high-resolution absorption spectra provided by the HITEMP2010.

Results showed that the error in the prediction can be as high as 24% for the maximum value of radiative heat source, although for carbon monoxide formation this value is lower than 7.0% for the cases presented.

Considering the diversity of cases presented, the formulation of the WSGG that presented a best result on average was the one that applies the superposition method that calculates separately the influence of water vapor and carbon dioxide.

6. ACKNOWLEDGEMENTS

Author GCF thanks the National Council for Scientific and Technological Development (CNPq) for a postdoctoral scholarship. FHRF thanks CNPq for research grant 302686/2017-7.

7. REFERENCES

Coelho, F. and França, F.H.R., 2019. "WSGG correlations based on HITEMP2010 for gas mixtures of H_2O and CO_2 in high total pressure conditions". *International Journal of Heat and Mass Transfer*, Vol. 127, pp. 105-114

de Goey, L.P.H. and Boonkkamp, J.H.M.T., 1999. "A flamelet description of premixed laminar flames and the relation with flame stretch". *Combustion and Flame*, Vol. 119, pp. 253-271.

Dorigon, L.J., Duciaki, G., Brittes, R., Cassol, F., Galarça, M. and França., F.H.R., 2013. "WSGG correlations based on HITEMP 2010 for computation of thermal radiation in non-isothermal, non-homogeneous H_2O/CO_2 mixtures". *International Journal of Heat and Mass Transfer*, Vol. 64, pp. 863–873.

Fraga, G.C., Zannoni, L., Centeno, F.R. and França, F.H.R., 2019. "Evaluation of different gray gas formulations against line-by-line calculations in two- and three-dimensional configurations for participating media composed by CO_2, H_2O and soot". *Fire Safety Journal*, Vol. 108.

Fraga, G.C., Bordbar, H., Hostikka, S. and França, F.H.R., 2020. "Benchmark Solutions of Three-Dimensional Radiative Transfer in Nongray Media Using Line-by-Line Integration". *Journal of Heat Transfer*, Vol. 142.

Goswami, M., 2014. *Laminar burning velocities at elevated pressures using the heat flux method*. Eindhoven University of Technology. https://doi.org/10.6100/IR766389

Howell, J.R., Menguç, M.P. and Siegel, R., 2016. *Thermal Radiation Heat Transfer*. Taylor & Francis Group, Florida, USA.

Kazakov, A. and Frenklach, M., 1995. *Reduced Reaction Sets based on GRI-Mech 1.2*. University of California at Berkeley. http://www.me.berkeley.edu/drm/

Krishnamoorthy, G., 2010. "A new weighted-sum-of-gray-gases model for CO_2-H_2O gas mixtures". *International Communications in Heat and Mass Transfer*, Vol 104, pp. 602-608.

Rothman, L.S., Gordon, I.E., Barber, R.J., Dothe, H., Gamache, R.R., Goldman., A., Perevalov, V., Tashkun, S.A., Tennyson, J. 2010. "HITEMP, the high-temperature molecular spectroscopic database". *Journal of Quantitative Spectroscopy and Radiative Transfer*, Vol. 111, pp. 2139–2150.

Smith, T.F., Shen, Z.F. and Friedman, J.N., 1982. "Evaluation of Coefficients for the Weighted Sum of Gray Gases Model". *Journal of Heat Transfer*, Vol 37, pp. 1182-1186.

Somers, B., 1994. *The simulation of flat flames with detailed and reduced chemical models.* Eindhoven University of Technology.

Yin, C., 2013. "Refined Weighted Sum of Gray Gases Model for Air-Fuel Combustion and Its Impacts". *Energy and Fuels*, Vol. 27, pp.-507-514.

8. RESPONSIBILITY NOTICE

The authors are the solely responsible for the printed material included in this paper.